Int. J. Electrochem. Sci., 11 **(2016)** 8810 – 8816, doi: 10.20964/2016.10.44

International Journal of
ELECTROCHEMICAL
SCIENCE
www.electrochemsci.org

Short Communication

Co_2P/rGO Nanoybrids as Advanced Electrocatalysts for Hydrogen Evolution Reaction

Yuan Hong, Weiguo Zhang, Zhenhai Wen, Suqin Ci[*]

Key Laboratory of Jiangxi Province for Persistent Pollutants Control and Resources Recycle, Nanchang Hangkong University, Nanchang 330063, PR China
[*]E-mail: cisuqin@gmail.com

Received: 10 May 2016 / *Accepted:* 12 August 2016 / *Published:* 6 September 2016

We herein report a simple and efficient hydrothermal method to prepare Co_2P nanoparticles loading on reduced graphene oxide composites (Co_2P/rGO). The morphology and structure of Co_2P/rGO composites were characterized by a variety of techniques, including X-ray diffractometer (XRD), scanning electron microscopy (SEM), transmission electron microscopy (TEM) and Brunauer-Emmett-Teller (BET). The Co_2P/rGO composites were investigated as electrocatalysts for hydrogen evolution reaction (HER), which show an outstanding electrocatalytic performance for HER with a low over-potential and a small Tafel slope.

Keywords: Co_2P, graphene, electrocatalyst, Hydrogen evolution reaction

1. INTRODUCTION

Nowadays, it is of great importance to develop electrochemical technology for generating hydrogen by the means of reduction of water, i.e. hydrogen evolution reaction (HER), such technique strongly depends on the catalytic performance of the catalysts [1-5]. So far, platinum (Pt) based catalyst is the most efficient electrocatalyst for HER, however, Pt is a well-known rare and expensive metal [6-10]. Therefore, it is very meaningful to explore low-cost and earth-abundant materials as alternative catalysts of Pt-based electrocatalyst [11].

Recently, transition metal phosphides (TMP) were regard as a class of potential electrocatalysts for HER due to their considerable activity upon catalyzing HER, such as molybdenum phosphide (MoP) [12, 13], nickel phosphide (Ni_2P) [14, 15] and Cobalt Phosphide Nanoparticles (Coop) [16]. For instance, it was reported that Ni_2P nanoparticles, a well-known hydrodesulfurization catalyst, showed an overpotential of -130 mV for 20 mA cm^{-2} in 0.5 M H_2SO_4[14]. Nevertheless, there is still great

room to advance the catalytic performance of TMP for HER. One promising strategy is to develop composite by loading TMP nanoparticles on graphene, in this way, the catalytic sites can be sufficiently activated by taking advantage of the favorable properties in graphene, including two-dimensional flexible structure, high electrical conductivity, and high surface area. Actually, a lot of metal oxide or hydroxide loading on graphene hybrids have been reported to promote their catalytic activity [17-19].

Bearing these points in mind, we herein report a one-step hydrothermal route to prepare reduced graphene oxide (rGO) supporting Co_2P hybrid (Co_2P/rGO) electrocatalyst for HER. We also confirmed that the catalytic activity is highly improved with a high current density, low overpotential and small Tafel slopes.

2. EXPERIMENTAL SECTION

2.1. Materials

All chemicals were analytical grade and were purchased from Xilong Chemical Co., Ltd. (Shantou, China). Nafion (5 wt.%) was purchased from Sigma-Aldrich. Pt/C (20 wt.%) was purchased from Alfa Aesar. Graphene oxide was prepared through a modified Hummer method. All solutions and electrolytes were freshly prepared with Milli-Q deionized (DI) water.

2.2. Synthesis of Co_2P/rGO and Co_2P

Co_2P was prepared through a minor modified method reported previously. Typically, 5.0 mM $Co(NO_3)_2 \cdot 6H_2O$ and 5.0 mM urea we added in 70 mL GO solution (~1.0 mg/mL) upon stirring until they are completely dissolved; then 5.0 mM red phosphorus powder were slowly added in the above solution with vigorous agitation with forming a red suspension, which was transferred to a 100 mL autoclave and kept at 200 °C for 20 h. The Co_2P/rGO solid products were obtained by thoroughly washing with distilled water, vacuum filtration, and drying at 60℃ for 3h. The synthesis process of Co_2P is similar to that of Co_2P/rGO just using pure water rather than GO solution.

2.3. Characterizations

The crystal structure, morphology, nanostructures and surface area were characterized by using an automatic X-ray diffractometer (XRD, Rigaku D/max 2200 PC) operated at 40 kV and 40 mA with Cu Kα radiation, a SSX-550 scanning electron microscopy (SEM, Shimadzu), Transmission electron microscopy (TEM, Hitachi H 9000 NAR) and N_2 sorption-desorption isotherms at 77 K using a Quantachrome NOVA 2000e adsorption apparatus, respectively.

2.4. Electrochemical Measurements

All electrochemical tests were performed in an electrochemical instrument (CHI760D, CHI Instrument) by using a traditional three-electrode system, in which a saturated Ag/AgCl electrode and a platinum sheet were served as reference and counter electrode, respectively, and modified glass carbon electrode (GCE) was used as working electrode. 5 mg electrode materials (Co_2P, Co_2P/rGO, and Pt/C) were scattered well in a mixture of 0.05 mL Nafion and 0.95 mL distilled water by ultrasonic agitation. Then, 6 μL of the mixture was dropped onto the surface of GCE that was pretreated by polishing using aluminum oxide (Al_2O_3, 0.3 μm) and cleaning *via* sonication; such modified electrode after drying in room temperature was used as working electrode. HER measurements were recorded in 0.5 M H_2SO_4 solution at room temperature by using cyclic voltammetry (CV) and linear sweep voltammetry (LSV). Electrochemical impedance spectroscopic (EIS) measurements were taken from 10^{-2} Hz to 10^{6} Hz.

3. RESULTS AND DISCUSSION

3.1. Characterisation of Co_2P/rGO nanocomposities

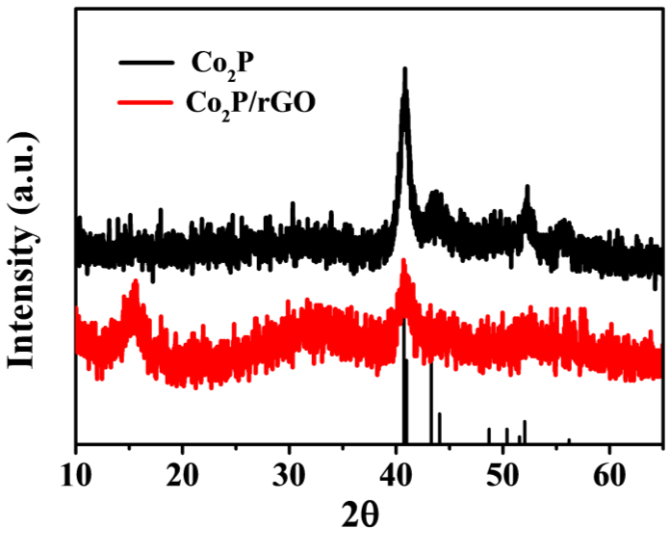

Figure 1. XRD patterns of products a) Co_2P; b) Co_2P/rGO.

Fig. 1 shows the powder XRD patterns of the as-produced Co_2P/rGO composite and bare Co_2P. Both samples show two peaks at 2θ=41.2° and 52.6°, which are well indexed as typical peaks of the standard Co_2P phase (JCPDS no. 32-0306) and consistent with other reports [20-22]. It should be noted that the peaks of Co_2P/rGO are slightly broader and weaker with respect to the bare Co_2P, indicating a lower crystallinity of Co_2P after loading on GO possibly because the introducing of GO result in forming a smaller Co_2P nanocrystalline, leading to the decrease of Co_2P XRD peaks in intensity and broadening of XRD peaks in width. Importantly, there is no characteristic diffraction peak of graphene, indicating that introduction of Co_2P nanoparticles effectively prevents restacking of rGO, which is consistent with the previous reports [23,24]. The peak at ~15° corresponds with red phosphorus resulting from residual reactant [25, 26].

The morphologies of the as-obtained Co_2P and Co_2P/rGO composite were characterized by SEM and TEM.

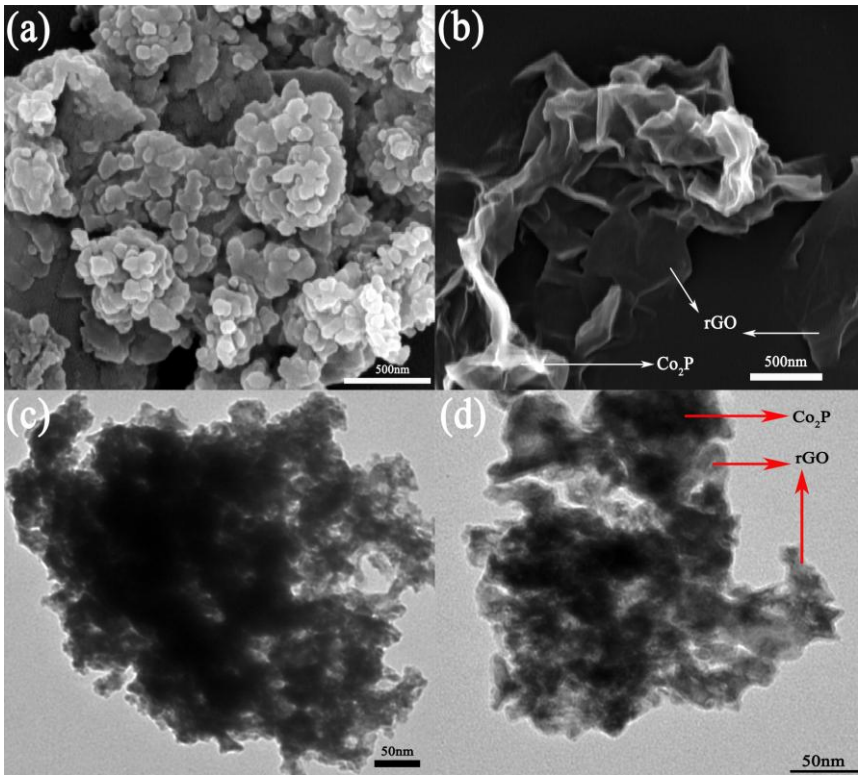

Figure 2. SEM images of a) Co_2P; b) Co_2P/rGO and TEM of c) Co_2P; d) Co_2P/rGO.

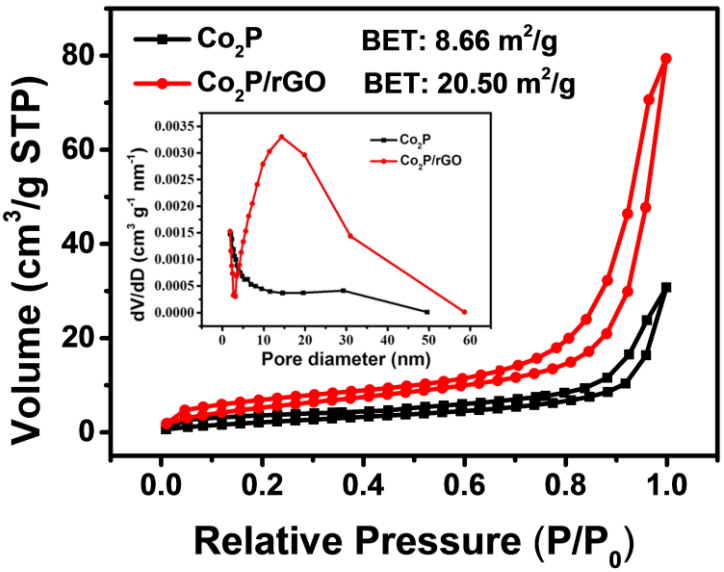

Figure 3. Corresponding nitrogen adsorption–desorption isotherm; inset shows the pore diameter distribution of Co_2P and Co_2P/rGO.

As shown in Fig. 2a and 2c, one can see Co_2P nanoparticles agglomerate together with formation of a microstructure, which may lead to a decrease of the catalytic active site for HER.

However, the Co_2P/rGO hybrid presents a folded flake structure, in which Co_2P nanoparticles are uniformly dispersed on graphene (Fig. 2b and Fig. 2d). We have the nitrogen adsorption-desorption isotherm and the pore size distribution curve of Co_2P and Co_2P/rGO illustrated in Fig. 3. The pore distribution of the two samples is calculated by using the BJH method from the desorption branch of the nitrogen isotherms. Remarkably, The BET surface areas of the Co_2P and Co_2P/rGO are 8.66 and 20.50 m^2 g^{-1} respectively.

3.2. Electrocatalytic activity of Co_2P/rGO toward HER

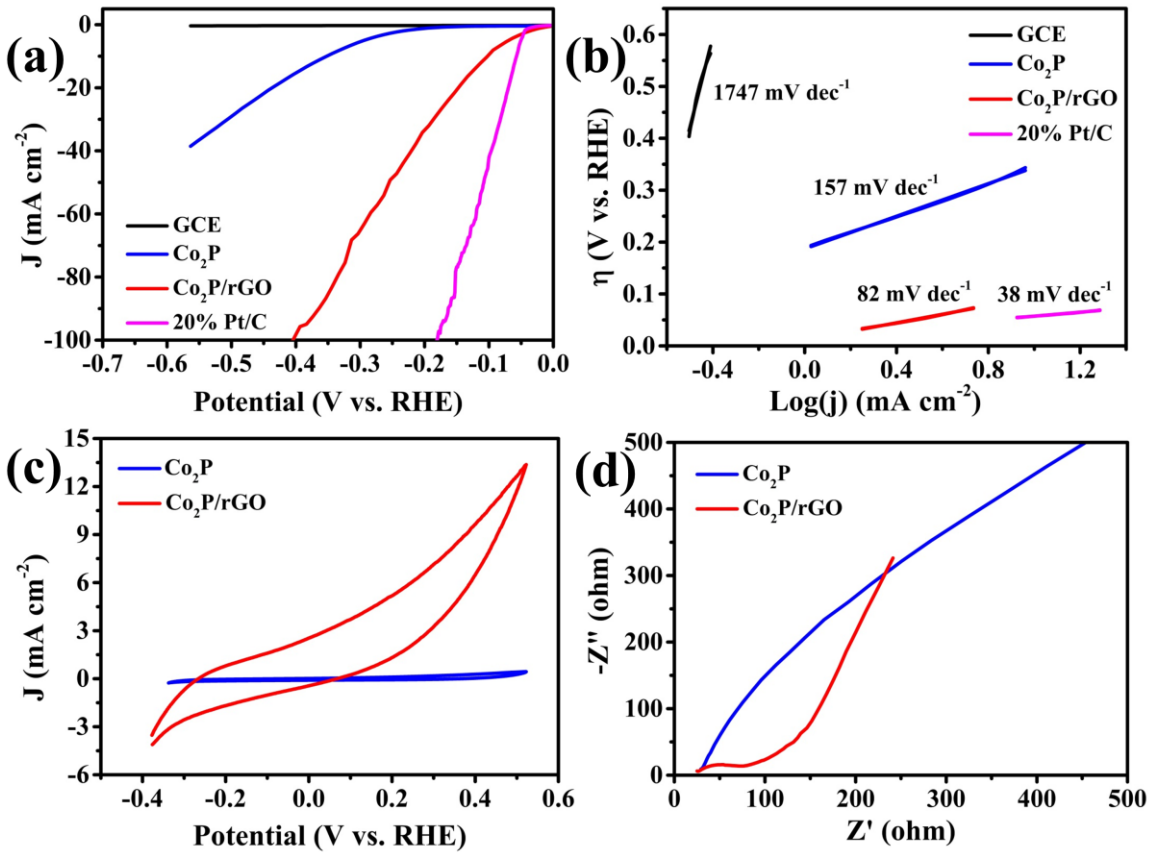

Figure 4. (a) Polarization curves, (b) corresponding Tafel plots, (c) Cyclic Voltammetry (CV), (d) Electrochemical impedance spectroscopic (EIS) of Co_2P and Co_2P/rGO.

The HER activities of the samples modified on glass carbon electrode(GCE) were performed in 0.5M H_2SO_4 solution in the potential range from 0.2V to -0.8 V (vs. Ag/AgCl) with the scan rate of 10 mV s^{-1}. Figure 4a shows the polarization curves of the current density (J) versus the potential of the bare GCE, Co_2P, Co_2P/rGO and and commercial Pt/C catalysts. As seen in the polarization curves, compared with the bare GCE, both Co_2P and Co_2P/rGO manifest more positive onset potential and much higher current density at the same potential. Upon a close observation, The Co_2P exhibits a overpotential of -440 mV at a cathodic current density of 20 mA cm^{-2} for a mass loading of 0.42 mg cm^{-2}. However, the Co_2P/rGO is -145 mV at a current density of 20 mA cm^{-2}($\eta_{-20\ mA\ cm-2}$= -145 mV),

suggesting a higher catalytic activity of the Co_2P/rGO for HER. Notably, the Co_2P/rGO exhibited a small difference in the onset potential relative to the commercial Pt/C catalyst, and the overpotential at 20 mA cm^{-2} is lower than some other efficient, earth-abundant HER electrocatalysts, such as Mo_2C on carbon nanotubes ($\eta_{-20\ mA\ cm-2}$ = -152 mV) [27] and MoS_2 ($\eta_{-20\ mA\ cm-2}$ = -175 mV) [28], comparable to those of Ni_2P ($\eta_{-20\ mA\ cm-2}$ = -130 mV) [14], and CoP($\eta_{-20\ mA\ cm-2}$ = -95 mV)[16], which have a mass loading of 0.9 mg cm^{-2}.

The Tafel plots of bare GCE, pristine Co_2P particles, Co_2P/rGO composites, and Pt/C derived from Fig.4a are shown in Fig.4b, in which a Tafel slope down to ~82 mV/decade was found for Co_2P/rGO according to the Tafel equation [29], which was much lower than those of previously reported other non-noble-metal HER catalysts, such as MoS_2 nanosheet (90 mV/decade), [30] hollow MoS_2 microspheres (125.2 mV/decade) [31], Ni_2P/graphene (82 mV/decade) [32] and CoP (104.8 mV/decade) [33]. To understand the electrochemical behavior under HER operating conditions, electrochemical impedance spectroscopy (EIS) were performed for the Co_2P/rGO hybrids and pristine Co_2P. Figure 2d shows the Nyquist plots for both catalysts, in which the observed semicircle is mainly attributed to the charge transfer resistance (R_{ct}) of H^+ reduction at the electrode-electrolyte interface. The Co_2P/rGO shows a charge transfer resistance of only about 50 Ω, much smaller than that of Co_2P, suggesting that the conductivity of the Co_2P/rGO is much higher than that of the Co_2P, which indicated a much faster electron transfer process during electrochemical reaction. Additionally, the electrochemically active surface area (EASA) of electrode corresponding to the activity of electrocatalysts is expressed by the loop curve area of the CV in Fig.4c, further confirmed that Co_2P/rGO own more catalytic sites than Co_2P. Thus, the positive shift of the onset potential, the decrease in overpotential at a current density of 20 mA cm^{-2} and the decreased Tafel slope strongly suggest the rGO could greatly enhance the catalytic activity of Co_2P. The enhanced electrocatalytic performance of Co_2P/rGO compared with that of Co_2P can be attributed to the strong chemical and electronic coupling between the rGO and the Co_2P, which leads to the larger accessible catalytic sites and the improved conductivity provided by CG, further indicating the rGO plays the important role in the electrocatalytic reduction of hydrogen. This hyperthesis was also confirmed by the previous studies [34, 35].

4. CONCLUSIONS

In conclusion, we have synthesized an efficient Co_2P/rGO electrocatalyst for hydrogen evolution via a facile hydrothermal approach. The Co_2P/rGO hybrid catalyst exhibited excellent HER activity affording current density of 20 mA cm^{-2} at the overpotential of ~145mV, and a Tafel slope as small as 82 mV/decade. In this way, the method of materials synthesis on graphene may be useful for production of large quantities of platinum-free HER catalysts.

ACKNOWLEDGEMENTS
This work was supported by Natural Science Foundation of China (50978132, 51178213, 51238002, 51272099, 51308278) and Department of Education Fund of Jiangxi Province (GJJ13506).

References

1. G. W. Crabtree, M. S. Dresselhaus, M. V. Buchanan, *Phys. Today*, 57(2004) 39.
2. J. A. Turner, *Science*, 305(2004) 972.
3. D. Das, T. N. Veziroğlu, *Int. J. Hydrogen Energy*, 26(2001) 13.
4. M. Ni, M. K. Leung, D. Y. Leung, K. Sumathy, *Renew. Sust. Energ. Rev*., 11(2007) 401.
5. A. Steinfeld, *Sol. Energy*, 78(2005) 603.
6. J. M. Bockris, E. Potter, *J. Electrochem. Soc*., 99(1952) 169.
7. J. Bockris, I. Ammar, A. Huq, *J. Phys. Chem*., 61(1957) 879.
8. A. Lasia, Handbook of fuel cells (2010).
9. H. Miao, D. Piron, *Electrochim. Acta*, 38(1993) 1079.
10. A. Walkley, *J. Electrochem. Soc*., 99(1952) 209C.
11. A. Chen, P. Holt-Hindle, *Chem. Rev*, 110(2010) 3767.
12. A. De Poulpiquet, H. Marques-Knopf, V. Wernert, M. T. Giudici-Orticoni, R. Gadiou, E. Lojou, *Phys Chem Chem Phys*, 16(2014) 1366.
13. X. Chen, D. Wang, Z. Wang, P. Zhou, Z. Wu, F. Jiang, *Chem. Commun*., 50(2014) 11683.
14. E. J. Popczun, J. R. Mckone, C. G. Read, A. J. Biacchi, A. M. Wiltrout, N. S. Lewis, R. E. Schaak, *J. Am. Chem. Soc*., 135(2013) 9267.
15. L. Feng, H. Vrubel, M. Bensimon, X. Hu, *Phys. Chem. Chem. Phys*., 16(2014) 5917.
16. E. J. Popczun, C. G. Read, C. W. Roske, N. S. Lewis, R. E. Schaak, *Angew. Chem*., 126(2014) 5531.
17. Y. Li, H. Wang, L. Xie, Y. Liang, G. Hong, H. Dai, *J. Am. Chem. Soc*., 133(2011) 7296.
18. B. Xia, Y. Yan, X. Wang, X. W. D. Lou, *Mater. Horiz*., 1(2014) 379.
19. E. Yoo, T. Okata, T. Akita, M. Kohyama, J. Nakamura, I. Honma, *Nano Lett*., 9(2009) 2255.
20. C. Han, X. Bo, Y. Zhang, M. Li, A. Wang, L. Guo, *Chem. Commun*., 51(2015) 15015.
21. Z. Jin, P. Li, D. Xiao, *Green Chem*. 18(2016) 1459.
22. J. F. Callejas, C. G. Read, E. J. Popczun, J. M. Mcenaney, R. E. Schaak, *Chem. Mater*., 27(2015) 3769.
23. S. Peng, L. Li, X. Han, W. Sun, M. Srinivasan, S. G. Mhaisalkar, F. Cheng, Q. Yan, J. Chen, S. Ramakrishna, *Angewandte Chemie*, 53(2014) 12594.
24. Q. Qu, S. Yang, X. Feng, *Adv Mater*, 23(2011) 5574.
25. W. J. Li, S. L. Chou, J. Z. Wang, H. K. Liu, S. X. Dou, *Nano Lett*, 13(2013) 5480.
26. R. Wu, D. P. Wang, X. Rui, B. Liu, K. Zhou, A. W. Law, Q. Yan, J. Wei, Z. Chen, *Adv. Mater*, 27(2015) 3038.
27. H. Vrubel, X. Hu, *Angew. Chem*., 124(2012) 12875.
28. W. Trakarnpruk, B. Seentrakoon, *Ind. Eng. Chem. Res*., 46(2007) 1874.
29. E. Gileadi, E. Kirowa-Eisner, *Corros. Sci*., 47(2005) 3068.
30. D. Merki, X. Hu, *Energy Environ. Sci*., 4(2011) 3878.
31. S. Muralikrishna, K. Manjunath, D. Samrat, V. Reddy, T. Ramakrishnappa, D. Nagaraju, RSC Adv, 5(2015) 89389.
32. B Dong, G-Q Han, W-H Hu, Y-R Liu, X Li, X Shang, Y-M Chai, Y. Q Liu, C. G. Liu, *Int. J. Electrochem. Sci*, 11(2016) 2846.
33. L. Ma, X. Shen, H. Zhou, G. Zhu, Z. Ji, K. Chen, *J. Mater. Chem*. A, 3(2015) 5337.
34. S. Mao, Z. H. Wen, S. Q. Ci, X. R. Guo, K. K. Ostrikov, J. H. Chen, *Small* 11(2014) 414.
35. Y. Li , H. Wang , L. Xie , Y. Liang , G. Hong , H. Dai , *J. Am. Chem. Soc*. 133(2011) 7296.